Available online at www.sciencedirect.com
ScienceDirect
Nuclear Physics B Proceedings Supplement 00 (2014) 1–15
Nuclear Physics B Proceedings Supplement

Precision top-quark physics with applications

M. Czakon

Institute for Theoretical Particle Physics and Cosmology, RWTH Aachen University, D-52056 Aachen, Germany

Abstract

We review the recent progress in the determination of top-quark pair production cross sections at hadron colliders, in particular the Tevatron and the LHC. We discuss the theoretical developments, which lead to the determination of next-to-next-to-leading (NNLO) corrections to this process. Furthermore, we describe some applications which follow from a comparison of theory predictions with data, e.g. the determination of the top-quark pole mass, constraints on the gluon distribution function and bounds on light top squarks. Finally, we present the most recent analysis of the Tevatron forward-backward asymmetry, where we demonstrate agreement between the Standard Model and the measurement.

Keywords:
top-quark, next-to-next-to-leading order QCD, subtraction schemes, parton distribution functions, supersymmetry

1. Introduction

Top-quark pair-production is one of the cornerstones of the Standard Model (SM) program at hadron colliders, and a number of precision calculations of this process have appeared in the recent past. In this proceedings, we focus our attention first and foremost on the total inclusive cross-section which, during the last two years, became known in full NNLO. This progress allowed for several non-trivial applications, and ultimately became the basis for high-precision predictions at the differential level. As an example of the latter, we discuss the top-quark forward-backward asymmetry as measured at the Tevatron.

The text is organised as follows. In the next section, we discuss the total cross section at fixed order and with resummation. We continue with a presentation of methods, which have been used for the determination of both real-radiation and virtual corrections. Subsequently, we discuss three applications: top-quark pole mass measurement, constraints on the gluon PDF, and bounds on top squarks. The last main section concerns the forward-backward asymmetry at the Tevatron. Short conclusions close the proceedings.

2. Total cross sections at fixed order and with resummation

The total top-pair production cross-section reads:

$$\sigma_{\rm tot} = \sum_{i,j} \int_0^{\beta_{\rm max}} d\beta\, \Phi_{ij}(\beta,\mu^2)\, \hat{\sigma}_{ij}(\beta, m^2, \mu^2)\,, \qquad (1)$$

where i, j run over all possible initial sate partons, Φ_{ij} is the partonic flux which is a convolution of the densities of partons i, j and includes a Jacobian factor

$$\Phi_{ij}(\beta,\mu^2) = \frac{2\beta}{1-\beta^2}\, \mathcal{L}_{ij}\left(\frac{1-\beta^2_{\rm max}}{1-\beta^2}, \mu^2\right), \qquad (2)$$

with

$$\mathcal{L}_{ij}(x,\mu^2) = x\left(f_i \otimes f_j\right)(x,\mu^2)\,, \qquad (3)$$

where $\otimes$ is defined as $(f \otimes g)(x) = \iint_0^1 {\rm d}y\, {\rm d}z\, f(y) g(z)\, \delta(x - yz)$. The dimensionless variable $\beta = \sqrt{1-\rho}$, with $\rho = 4m^2/s$, is the relative velocity of the final state top quarks having pole mass m and produced at partonic c.m. energy $\sqrt{s}$; $\beta_{\rm max}$ corresponds to the collider c.m. energy; μ stands for

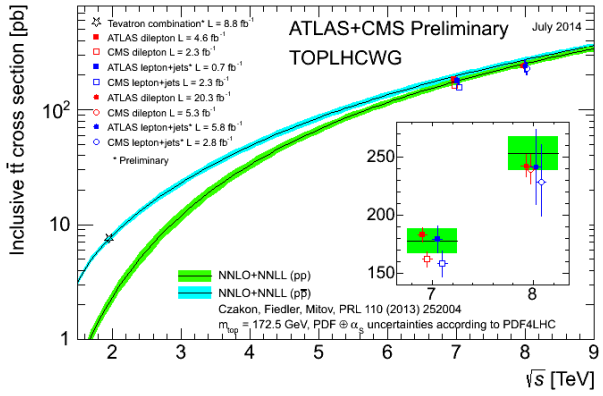

Figure 1: *Summary of LHC and Tevatron measurements of the top-quark-pair production cross section as a function of the centre-of-mass energy compared to the NNLO QCD calculation complemented with NNLL resummation (top++2.0). The theory band represents uncertainties due to renormalisation and factorisation scale, parton density functions and the strong coupling. The measurements and the theory calculation are quoted at $m_t = 172.5$ GeV. Measurements made at the same centre-of-mass energy are slightly offset for clarity. Plot taken from [16].*

both the renormalization (μ_R) and factorization scales (μ_F).

For $\mu_F = \mu_R = \mu$ the partonic cross-section reads:

$$\hat{\sigma}_{ij}\left(\beta, m^2, \mu^2\right) = \frac{\alpha_S^2}{m^2}\left\{\sigma_{ij}^{(0)} + \alpha_S\left[\sigma_{ij}^{(1)} + L\,\sigma_{ij}^{(1,1)}\right] + \alpha_S^2\left[\sigma_{ij}^{(2)} + L\,\sigma_{ij}^{(2,1)} + L^2\sigma_{ij}^{(2,2)}\right] + O(\alpha_S^3)\right\}, \quad (4)$$

where $L = \ln\left(\mu^2/m^2\right)$ and α_S is the $\overline{\text{MS}}$ coupling renormalized with $N_L = 5$ active flavors at scale μ^2. The functions $\sigma_{ij}^{(n(,m))}$ depend only on β.

The dependence on $\mu_R \neq \mu_F$ can be trivially restored in Eq. (4). The NLO results are known exactly [1, 2, 3]. The scale controlling functions $\sigma_{ij}^{(2,1)}$ and $\sigma_{ij}^{(2,2)}$ can be easily computed from the NLO results $\sigma_{ij}^{(1)}$, and can be found in [4]. The fixed order results at NNLO have been calculated in a series of papers [5, 6, 7, 8]. Augmented with next-to-next-to-leading logarithmic resummation of soft gluon effects [9, 10, 11], these results have been implemented in the C++ program Top++ [12]. Figure 1 presents a comparison between the most recent data and the best theory predictions. We note that prior to the exact NNLO results, the most precise theory understanding of the total cross section was based on its expansion in the threshold limit [13].

The results of Refs. [5, 6, 7, 8] have been obtained with numerical methods discussed in the next section. They are given in the form of fitting formulae as a polynomial in the number of active flavors

$$\sigma_{ij}^{(2)}(\beta) = F_0^{ij}(\beta) + F_1^{ij}(\beta)N_L + F_2^{ij}(\beta)N_L^2\,. \quad (5)$$

The functions F_2^{ij} do not present any threshold enhancements. On the other hand, both $F_{0,1}^{q\bar{q}}$ and $F_{0,1}^{gg}$ are affected by soft-gluon and Coulomb effects at $\beta = 0$. These are known analytically in a power-logarithmic expansion [13]. The difference between the exact result and the analytic threshold expansion, $F_{0,1}^{(\text{fit})}$ is shown in Figs. 2 and 3. Fig. 3 also contains $F_2^{(\text{fit})}$ for the gluon fusion channel, since the latter could not be obtained in closed analytic form.

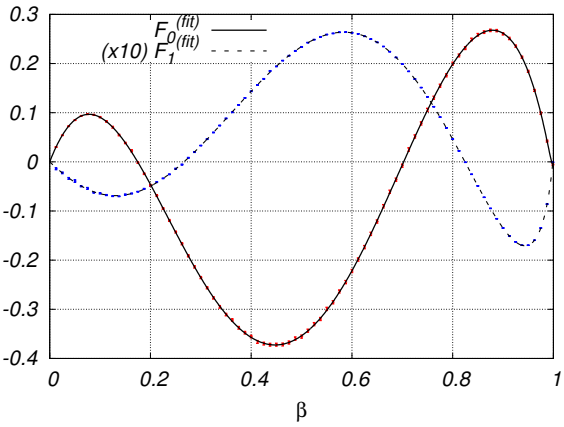

Figure 2: *The functions $F_0^{(\text{fit})}$ and $10 \times F_1^{(\text{fit})}$ (rescaled for improved visibility) for the $q\bar{q}$ channel as: a) discrete sets of calculated values, with errors, on the grid of 80 points (red and blue error bars - barely visible because of the size of the errors) and b) analytical fits (black lines). Plot taken from [5].*

The exact calculation of the NNLO corrections allowed for a very precise determination of the total cross section. Table 1 gives the values for various colliders. It contains an account of the error estimates due to the theory uncertainty as obtained from scale variation and input parameter variation, in particular the dependence on the parton distribution functions. We notice that the intrinsic uncertainty of the theory is at the level of 5%, whereas that due to PDFs is lower, at the level of 3%. It turns out that soft gluon resummation allows to further reduce the theory uncertainty, while at the same time slightly increasing the prediction. The respective values are given in Tab. 2. The quoted theory precision is at the level of 3%. We note that the known electroweak corrections [14, 15] for this process are negligible on this

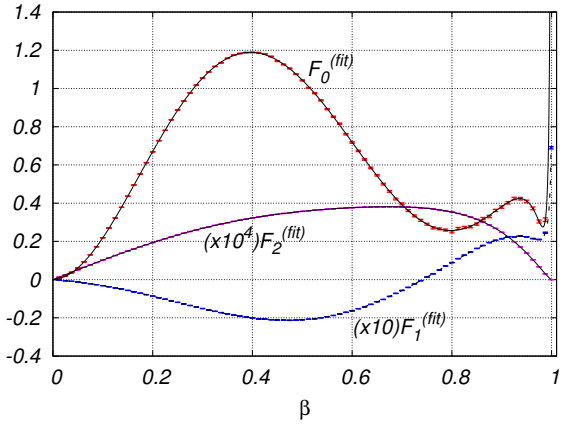

Figure 3: *The functions $F^{(\mathrm{fit})}_{2,1,0}$ for the gg channel versus the 80 computed points. For improved visibility, the function $F^{(\mathrm{fit})}_1$ is multiplied by a factor of 10, while $F^{(\mathrm{fit})}_2$ by a factor of 10^4. Plot taken from [8].*

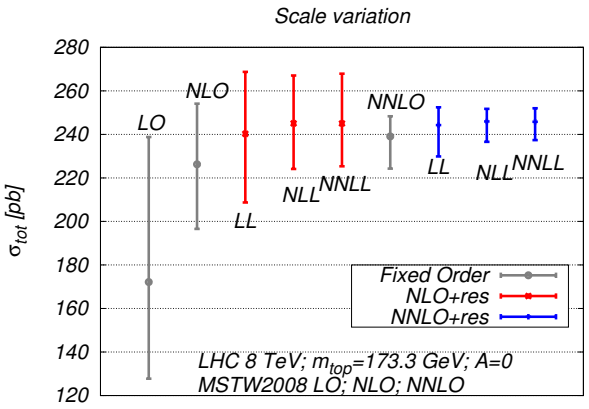

Figure 4: *Convergence of the perturbative expansion [17] of the total top-quark pair production cross section, including scale variation. The predictions correspond to the LHC @ 8 TeV. The parameter A set to 0 in this plot pertains to sub-leading effects in soft-gluon resummation (see Ref. [11]).*

scale. On the other hand, it is currently hardly imaginable to further reduce the theory uncertainty. This would, in fact, require a calculation of QCD corrections at the N^{3}LO. In any case, it is interesting to observe that top-quark production exhibits a good perturbative expansion. This is illustrated in Fig. 4.

Collider	σ_{tot} [pb]	scales [pb]	pdf [pb]
Tevatron	7.009	$^{+0.259(3.7\%)}_{-0.374(5.3\%)}$	$^{+0.169(2.4\%)}_{-0.121(1.7\%)}$
LHC 7 TeV	167.0	$^{+6.7(4.0\%)}_{-10.7(6.4\%)}$	$^{+4.6(2.8\%)}_{-4.7(2.8\%)}$
LHC 8 TeV	239.1	$^{+9.2(3.9\%)}_{-14.8(6.2\%)}$	$^{+6.1(2.5\%)}_{-6.2(2.6\%)}$
LHC 14 TeV	933.0	$^{+31.8(3.4\%)}_{-51.0(5.5\%)}$	$^{+16.1(1.7\%)}_{-17.6(1.9\%)}$

Table 1: *Pure NNLO theoretical predictions [8] for various colliders and c.m. energies.*

Collider	σ_{tot} [pb]	scales [pb]	pdf [pb]
Tevatron	7.164	$^{+0.110(1.5\%)}_{-0.200(2.8\%)}$	$^{+0.169(2.4\%)}_{-0.122(1.7\%)}$
LHC 7 TeV	172.0	$^{+4.4(2.6\%)}_{-5.8(3.4\%)}$	$^{+4.7(2.7\%)}_{-4.8(2.8\%)}$
LHC 8 TeV	245.8	$^{+6.2(2.5\%)}_{-8.4(3.4\%)}$	$^{+6.2(2.5\%)}_{-6.4(2.6\%)}$
LHC 14 TeV	953.6	$^{+22.7(2.4\%)}_{-33.9(3.6\%)}$	$^{+16.2(1.7\%)}_{-17.8(1.9\%)}$

Table 2: *Best NNLO+NNLL theoretical predictions [8] for various colliders and c.m. energies.*

An important goal of the publications [5, 6, 7, 8] was to assess the precision of various previous approximations to the QCD corrections to the hadronic cross section. Most of these were based on soft-gluon resummation, e.g. as studied in Ref. [11]. It was possible to show that the sub-leading terms in the threshold expansion, which can only be determined in an exact calculation, have a noticeable impact on the final prediction. It turned out, for example, that in the case of the LHC setup the difference between the exact result and previous approximations reached up to 12%, which is the same size as the total NNLO correction itself. The source of such large discrepancies is best illustrated by comparing the analytic expansion with the exact result multiplied by the parton flux in the gluon case. This is shown in Fig. 5. It is seen that while the results coincide in the threshold region $\beta \approx 0$, there is a difference over most of the β variation range, which is further enhanced by the large gluon flux.

Another approximation method has been proposed in [18]. The idea of that publication was to use Padé approximants linking the threshold region with the high-energy region to cover the complete variation range of β. The quality of this approach can be illustrated in the case of the quark-gluon channel [7]. The most prominent feature of the partonic cross-section $\sigma^{(2)}_{qg}$ is its high-energy behavior [1, 19, 20, 21, 22, 23]

$$\sigma^{(2)}_{qg\to t\bar{t}+X}\Big|_{\rho\to 0} \approx c_1 \ln(\rho) + c_0 + O(\rho)\,. \tag{6}$$

The constant c_1 has been predicted exactly in Ref. [24], with an N_L-independent numerical value

$$c_1 = -1.689571450230512\,. \tag{7}$$

To improve the high-energy endpoint behavior of the

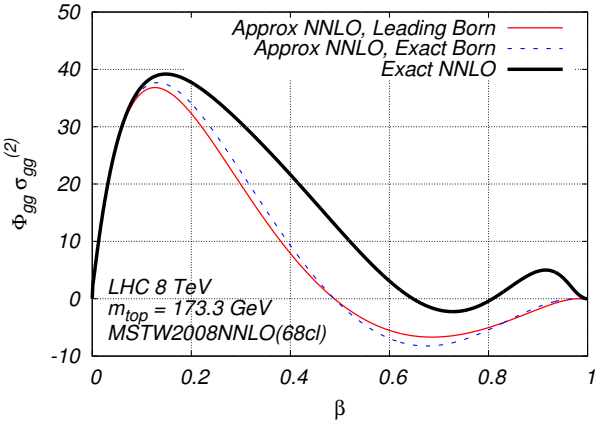

Figure 5: *Partonic cross-section times gg flux (2) for the following three cases: exact NNLO (thick black line), approximate NNLO with exact Born term (blue dashed line) and approximate NNLO with leading Born term (thin red line). The plot is reproduced after Ref. [8].*

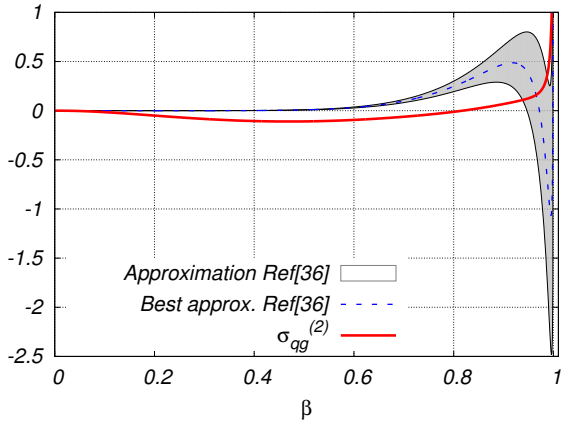

Figure 6: *Comparison [7] of the exact partonic cross-section $\sigma_{qg}^{(2)}$ (solid red) with the approximation of Ref. [18] (grey band, cited as Ref. [36] after the original publication Ref. [7]). The central value (dashed blue) is the "best" approximation of Ref. [18]. The approximation and the exact result have the same limit at $\beta \to 1$.*

fits, the exact $\sim \ln(\rho)$ behavior from (6) was imposed in Ref. [7]. Then, an estimate of the constant c_0 could be derived

$$c_0 = -9.96 + 0.0345 N_L \,. \tag{8}$$

Setting $N_L = 5$, Eq. (8) agrees [1] with the numerical estimate of c_0 derived in Ref. [18] with the help of completely independent methods. The success of the determination of the high energy behaviour does not, however, translate to a good estimate of the shape of the partonic cross section. This is demonstrated in Fig. 6. The origin of the large discrepancy lies in the choice of variable to perform the Padé approximation. As function of β (or ρ) the cross section is extremely sensitive to the order of expansion. Indeed, the difference between the leading behaviour and the complete high-energy expansion is very large already at NLO [3]. Thus, using only the leading behaviour at NNLO, one cannot expect to obtain a good approximation to the real behaviour of the function. For the total cross section, this approach causes differences with respect to the exact result at the level of almost 5%.

3. Perturbative methods

The results discussed in the previous section have been obtained from a next-to-next-to-leading order calculation of all the available partonic channels. NNLO calculations always involve the determination of the two-loop virtual, one-loop squared, real-virtual and double-real corrections. In our case, the two-loop virtual corrections have been evaluated as in Refs. [25, 26], utilising the analytical form for the poles [27]. The one-loop squared amplitude has been calculated previously [28, 29, 30] and confirmed by us. The real-virtual corrections have been derived by integrating the one-loop amplitude with a counter-term that regulates all its singular limits [31, 32, 33, 34]. The finite part of the one-loop amplitude has been computed with a code used in the calculation of $pp \to t\bar{t}j$ at NLO [35, 36]. The double real corrections have been computed as in Refs. [37, 38].

In this section, we would like to discuss the most challenging parts of the calculation, namely the evaluation of phase space integrals for real radiation and the determination of the two-loop virtual corrections. It turns out, for instance, that a method that has been proposed by us for the calculation of real radiation in top-quark pair production could be generalised and has already found many non-trivial applications. In fact, recently, we have been able to present a complete formulation for the calculation of arbitrary cross sections at NNLO.

3.1. Sector-improved residue subtraction scheme

A major obstacle in the calculation of NNLO corrections is the evaluation of double-real and mixed real-virtual contributions containing infrared singular phase space integrals. In principle, these contributions can be obtained by means of Monte Carlo techniques, once

[1] We note that the prediction for the constant c_0 derived in Ref. [18] contains no explicit N_L dependence.

suitable subtractions have been introduced to generate numerically integrable functions. The form of the subtractions defines a *subtraction scheme*. Unfortunately, it turns out that subtraction schemes are extremely complex. At present, there are several on-going multi-year efforts at the construction of general solutions. Antenna subtraction [39], and q_T subtraction [40], are amongst the most advanced initiatives, which have already found several non-trivial applications. Another scheme under construction has been introduced in Ref. [41]. Here, we will be concerned with the subtraction scheme STRIPPER introduced by us in Ref. [37]. Inspired in some aspects by ideas of Frixione, Kunszt and Signer [42], and in other aspects by ideas of Binoth and Heinrich [43] (see Ref. [44] as well), the scheme has proven its worth in many applications: it has allowed for the determination of NNLO corrections to hadronic top-quark pair production [38, 5, 6, 7, 8], fully differential top-quark decays [45], inclusive semileptonic charmless b-quark decays [46], associated Higgs boson and jet production in gluon fusion [47], muon decay spin asymmetry [48], and t-channel single-top production [49]. The listed advanced STRIPPER applications performed independently of the inventor have been preceded by the much simpler case of QED corrections to Z-boson decay into a pair of massless leptons [50]. The most recent work on the scheme [51] was concerned with completing the construction of the scheme in order to allow for the evaluation of cross sections for arbitrary processes.

The original idea of Ref. [37] was to concentrate on the numerical calculation of the coefficients of the Laurent expansion in ϵ (dimensional regularization parameter, with space-time dimension $d = 4-2\epsilon$) of the double-real cross section contribution. The latter requires a phase space integral over the momenta not only of the partons present in the Born approximation, but also of two additional massless partons. It seemed obvious that other cross section contributions are much easier to obtain, since their kinematics is, in the worst case, the same as that of next-to-leading order real-radiation contributions. Furthermore, the concept was to refrain from (almost) any analytic integration. By inspection of other efforts, it was clear that it is the insistence on analytic integration that makes the subtraction schemes difficult to develop. Finally, in order to avoid as many complications as possible, the construction was performed uniformly in d dimensions. This corresponds to conventional dimensional regularization, where both momenta and spin degrees-of-freedom of external particles are d dimensional. This implies that even Born matrix elements will have a non-trivial expansion in ϵ. While the other basic ideas of the scheme stood the test of time, the use of CDR is now an important drawback. Indeed, software implementations of tree-level matrix elements only provide them at $\epsilon = 0$, i.e. in four dimensions. This makes it necessary to recalculate the matrix elements for each project from scratch. Furthermore, the need to parameterize an increasing number of dimensions depending on the multiplicity of the process seems not only a major annoyance, but also a source of inefficiency. In the publication [51], the problem was solved by introducing a number of corrections to the integrated subtraction terms in the double-real radiation contribution. As a result, we have formulated the scheme in 't Hooft-Veltman regularization. In particular, we now only need four-dimensional external momenta and polarizations in the evaluation of actual matrix elements. There is still a trace of higher dimensionality in the integration over unresolved momenta. However, we only have to consider six dimensional unresolved momenta in the worst case. On the example of top-quark pair production, we have also demonstrated that the introduced improvements of STRIPPER fulfill their purpose. We stress that we have only presented the algorithm to obtain the expressions needed for the implementation of the subtraction scheme. This algorithm requires the knowledge of soft and collinear limits of QCD amplitudes and provides the expressions for the subtraction and integrated subtraction terms by simple substitutions. Due to the number and size of the resulting final formulae, we did not reproduce them in [51]. Instead, we plan to provide a software package in the future. Nevertheless, existing calculations can be converted to 't Hooft-Veltman regularization with moderate effort following Ref. [51].

As already mentioned, the idea behind the construction of the subtraction scheme STRIPPER is to derive Laurent expansions in ϵ for each of the cross section contributions independently. The basic algorithm has three stages:

phase space decomposition: phase spaces with $n + 1$ and $n + 2$ final-state particles (n being the number of particles at Born level) are decomposed into sectors, in which only certain types of singularities may occur;

phase space parameterization: in each sector, a special parameterization is introduced using spherical coordinates in d dimensions, in which singularities are only parameterized with 2 variables for $n + 1$-final-state-particles phase spaces, and with 4 variables for $n + 2$-final-state-particles phase spaces;

subtraction and integrated subtraction terms: in each parameterization, subtraction terms in the

relevant variables are introduced, which make it possible to obtain an expansion in ϵ, the coefficients of which are integrable. The subtraction terms only require the knowledge of the singular limits of QCD amplitudes, and are process independent in the sense that the process dependence is confined to the matrix elements. Furthermore, pointwise convergence of phase space integration is guaranteed.

After application of this algorithm, cross sections may in principle be evaluated numerically. Nevertheless, since dimensional regularization involves infinite dimensional vectors, the effective dimension of the vectors, which actually occur in the calculation increases with multiplicity. In fact, any new vector requires an increase of the effective dimension by one. For two-to-two processes at leading order, one already needs five dimensions at next-to-next-to-leading order. Furthermore, matrix elements must be provided as expansions in ϵ. In order to simplify the calculation, we introduce the 't Hooft-Veltman version of dimensional regularization, in which resolved particle momenta and spin degrees-of-freedom are four-dimensional. In this case, we also only need four-dimensional matrix elements. The construction proceeds in additional three stages:

average over azimuthal angles: integrated subtraction terms, which have been derived in relation to a collinear limit, are averaged over the unphysical transverse direction. For most cases, this is equivalent to the use of averaged splitting functions, but there are important exceptions. This step is important in order not to have contractions of four-dimensional matrix elements with d-dimensional transverse vectors;

separation of finite contributions: the different contributions listed in this section are further decomposed into classes with different kinematics and loop order. The sum of the terms in each class is finite. This requires a modification of the integrated subtraction terms for the double-real radiation. In practice, counterterms are introduced, which are added to one class of contributions and subtracted from another;

't Hooft-Veltman regularization: the measurement function is modified to contain delta-functions restricting the momenta of resolved particles to be four-dimensional. For most classes of finite contributions, this is already sufficient to fulfill the requirements of 't Hooft-Veltman regularization, and the matrix elements can be evaluated in four dimensions. Nevertheless, one class, the single-unresolved contributions to double-real radiation, requires a further modification of the integrated subtraction terms.

After these steps, the subtraction scheme does not require higher orders of the ϵ-expansion of the matrix elements, and all resolved momenta are four-dimensional. The calculation still involves unresolved momenta, which may need up to two additional dimensions, but only occur in soft and splitting functions. In general, two-to-two processes at leading order require five-dimensional unresolved momenta at next-to-next-to-leading order. For higher multiplicity, six-dimensional momenta must be introduced.

We will not give any further details of the complete formulation of the subtraction scheme from Ref. [51], since this would exceed by far the space foreseen for this proceedings. On the other hand, we will now discuss a comparison between results obtained using the CDR and 't Hooft-Veltman formulations for the particular case $gg \to t\bar{t} + ng$, $n = 0, 1, 2$.

The relevant partonic cross section is rendered dimensionless and independent of the value of the strong coupling with the normalization

$$\tilde{\sigma}^{(2)} = \frac{m_t^2}{\alpha_S^4}\hat{\sigma}^{(2)} \,, \tag{9}$$

where $\hat{\sigma}^{(2)}$ is the total cross section contribution at $O(\alpha_S^4)$. Furthermore, we set

$$\mu_R = \mu_F = m_t \,. \tag{10}$$

Our results are obtained at the point

$$\beta = \sqrt{1 - \frac{4m_t^2}{\hat{s}}} = 0.5 \,. \tag{11}$$

The cross section contributions are divided into double-unresolved and single-unresolved. The double-unresolved contributions correspond to coefficients of the poles in ϵ involving matrix elements with only four partons, in this case for the process $gg \to t\bar{t}$. We obtain

$$\tilde{\sigma}_{\rm DU}^{\rm CDR} = -0.0304(4) \,, \tag{12}$$

$$\tilde{\sigma}_{\rm DU}^{\rm HV} = -0.0304(2) \,. \tag{13}$$

Similarly, the single-unresolved contributions correspond to the coefficients of the poles in ϵ involving matrix elements with five partons, in this case for the process $gg \to t\bar{t}g$. These require subtraction terms, which

are also included. We obtain

$$\tilde{\sigma}_{\rm SU}^{\rm CDR} = 0.2506(3)\,, \tag{14}$$

$$\tilde{\sigma}_{\rm SU}^{\rm HV} = 0.2511(2)\,. \tag{15}$$

The agreement, up to statistical errors due to Monte Carlo integration, between the different evaluations serves as an excellent check of the correctness of the proposed approach.

3.2. Numerical methods for virtual corrections

The solution developed for the determination of real-radiation contributions to top-quark pair production at NNLO turned out be general and applicable to arbitrary processes as discussed in the previous sub-section. The case of the two-loop virtual corrections is more complicated. These contributions are still obtained on a process-by-process basis. There is a long-term effort to determine the amplitudes for top-quark pair production analytically [52, 53, 54, 55, 56]. We, on the other hand, decided to work with semi-numerical methods based on differential equations, as proposed in Ref. [25] and applied to the quark-annihilation channel. Instead of solving the differential equations analytically, the idea was to resort to numerical methods. The problems of this approach are of two kinds. At first, it is necessary to provide a boundary condition in the form of high precision values of the integrals at a single point. Inspired by Refs. [57, 58], a point in the high-energy range has been chosen for this purpose. The asymptotics of the integrals in this limit have been derived using Mellin-Barnes techniques. The second problem is related to singularities of the differential equations, which cause substantial problems. In the case of the quark-annihilation channel amplitudes, the use of higher numerical precision was sufficient to provide numerical values within some acceptable kinematical domain. Unfortunately, the gluon fusion channel is substantially more demanding both in the determination of the asymptotics of the integrals, and in the treatment of numerical instabilities. The techniques that we have applied in this case are discussed below. The results have been presented in [26].

The two-loop amplitudes for heavy-quark pair-production are expressed through 726 Feynman diagrams in the gluon-fusion channel, and 190 diagrams in the quark annihilation channel. Due to the structure of the QCD vertices, the topologies present in the quark-annihilation case are a subset of those present in the gluon case. Using the Laporta algorithm, the occurring integrals are reduced to a set of 422 masters, out of which only 145 are needed for the quark-annihilation case. Based on experience, we consider integrals with less than six propagators as easy. This leaves 212 difficult six and seven line integrals to evaluate. In our work, we did not use any external input, i.e. we did not rely on integrals calculated by others. Nevertheless, 38 of the difficult integrals have been evaluated by us in Ref. [25]. The remaining number is further reduced by the fact that 89 integrals can be obtained from others by a $t \leftrightarrow u$ channel transformation. Thus, the final number of new integrals that were evaluated in [26] was 100. Thanks to the work Ref. [58], 17 of these were at least known in the high-energy limit.

Since we are dealing with four-point amplitudes with a single mass scale, the integrals, M_i, once stripped of their global mass dimension by appropriate rescaling, depend on two dimensionless variables. This means that the functional dependence of the integrals is fully specified by two systems of homogeneous linear first order partial differential equations (s and t are the usual Mandelstam invariants, and m is the top-quark mass)

$$m^2\frac{\partial}{\partial m^2}M_i(m^2/s,\,t/s,\,\epsilon) = \sum_j J_{ij}^{(m^2)}(m^2/s,\,t/s,\,\epsilon)\,M_j(m^2/s,\,t/s,\,\epsilon)\,, \tag{16}$$

$$t\frac{\partial}{\partial t}M_i(m^2/s,\,t/s,\,\epsilon) = \sum_j J_{ij}^{(t)}(m^2/s,\,t/s,\,\epsilon)\,M_j(m^2/s,\,t/s,\,\epsilon)\,, \tag{17}$$

which can be obtained by taking derivatives in the parameters and reducing the resulting integrals with integration-by-parts identities to the original masters. The elements of the Jacobi matrices, $J^{(m^2)}$ and $J^{(t)}$, are rational functions of m^2/s, t/s and ϵ. We require a solution for the master integrals in the form of Laurent expansions in ϵ.

The solution of the system is obtained by choosing a path, possibly complex, in the parameter space

$$(m^2/s,\,t/s) \;\to\; (m^2(z)/s,\,t(z)/s)\,, \tag{18}$$

and solving the resulting ordinary differential equation in z. This can be done either numerically or as a power-logarithmic series in z. In practice, we have proceeded as follows

1. We have determined analytically the first few terms of the high-energy expansion of the master integrals. The results are a power-logarithmic series in m^2/s, with coefficients, which are exact in t/s. In

order to obtain our results, we have used Mellin-Barnes techniques, and in particular relied heavily on the MB package [59]. In a few cases, we recovered the exact dependence on t starting from the limiting behavior at $t = 0$ and using differential equations in t. In order to obtain the boundary condition, we performed a double expansion of the Mellin-Barnes representation of a given Feynman integral in m^2 and t. The resulting Mellin-Barnes integrals, which were pure numbers were evaluated with very high precision and resummed with the PSLQ algorithm [60]. In simpler cases, we have used the XSummer package [61] for resummation.

2. In a next step, we have obtained deep high-energy expansions using the differential equations in m^2 and the boundary conditions from the previous step. These expansions were used to derive high-energy expansions of the amplitudes, and to obtain high precision numerical values of the master integrals at small mass.
3. Using the numerical values determined in the previous step, we have solved the differential equations in m^2 and t along contours in the complex plane. To obtain the solution, we have used the software from Ref. [62] with improvements to handle higher precision numbers [63].
4. Around $\beta = 0$, we have obtained, with the help of the differential equations, deep power-logarithmic expansions in β for fixed values of the scattering angle. These expansions were generated from unknown boundary coefficients, which were determined by matching the expansion to the numerical solution from the previous step at a point, at which both the expansion and the numerical solution provide high precision. This method can be used at any singular point, and allows to avoid numerical instabilities of the differential equations.

The results obtained with this method fall into three kinematical domains: threshold, "bulk", and high-energy. The "bulk" domain covers moderate β values and is given purely numerically on a large grid. The sampling values of β are chosen as in [5, 6, 7, 8], i.e.

$$\beta_i = i/80 \,, \quad i = 1, ..., 79 \,, \tag{19}$$

and $\beta_{80} = 0.999$. This covers the range of values available at LHC @ 8 TeV. The dependence on the scattering angle is described through

$$\cos\theta_i = \pm x_i \,, \quad i = 1, ..., 21 \,, \tag{20}$$

where the x_i correspond to the 21 sampling points of the Gauss-Kronrod integration rule of order 10, and can be obtained with any major algebraic/numeric computer system, e.g. Mathematica. The Gauss-Kronrod rule is an efficient deterministic rule for smooth functions, which also provides an error estimate by sampling every second point of the rule with appropriate weights. This specific choice of the $\cos\theta$ points has been made, because a first aim was to provide very precise values of the contributions of the amplitudes to the total cross sections.

An example result is shown in Fig. 7 for the case of the gluon fusion channel with the number of light quarks set to zero. The main purpose of this figure is to demonstrate that, besides singularities at threshold and at high-energy forward and backward directions, the result is rather structureless. This allows in fact to use interpolation in practical implementations.

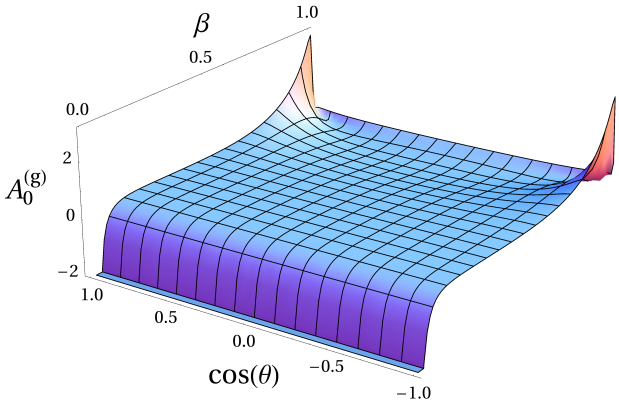

Figure 7: *Finite remainder of the gluon-fusion channel renormalized two-loop virtual amplitude for $N_L = 0$. The scale has been set to $\mu = m$. Plot taken from Ref. [26].*

Our results for the two-loop virtual amplitudes can be used to obtain the leading threshold behavior of partonic top-quark pair-production cross sections at next-to-next-to-leading order. When $\beta \approx 0$, cross sections are dominated by terms of the form $\beta \times 1/\beta^n \ln^m \beta$ with $n > 0$ and/or $m > 0$. While the first factor of β is a phase space suppression, the enhancements by positive powers of $\ln\beta$ and $1/\beta$ are due to emissions of soft gluons and non-relativistic potential interactions between the quark and the anti-quark. At next-to-next-to-leading order, the coefficients of these singular terms have been determined in Ref. [13]. In Ref. [26], we have extended the analysis to include terms with $n = m = 0$, which are velocity independent with respect to the Born cross section. The threshold expansion including both singular and constant terms can be obtained from factorization as explained in Ref. [64]. According to the latter pub-

lication, close to threshold, a cross section for a given initial state can be written as

$$\hat{\sigma} = \sum_{\alpha} H_{\alpha} \otimes S_{\alpha} \, . \tag{21}$$

H_{α} are called hard functions, and are obtained by expanding in β the partonic cross sections obtained exclusively with the finite remainder of the virtual amplitudes projected onto the color configuration α. Therefore, H_{α} do not contain any real-radiation effects. S_{α} are called soft functions, and are given by cross sections for emission of gluons and light-quark pairs from eikonal lines representing the external partons of the hard process in the color configuration α. The convolution is performed in the energy of the soft radiation. The color configurations, α, must correspond to irreducible representations of the SU(3) group, in order for this simple form to be valid.

Using Eq. (21), we have obtained [26] the following expansion for the gluon channel

$$\begin{aligned}\sigma^{(2)}_{gg} = {} & \frac{68.5471}{\beta^2} \\ & + \frac{1}{\beta}\Big(496.3\ln^2\beta + 321.137\ln\beta - 8.62261\Big) \\ & + 4608\ln^4\beta - 1894.91\ln^3\beta - 912.349\ln^2\beta \\ & + 2456.74\ln\beta + C^{(2)}_{gg} \, , \end{aligned} \tag{22}$$

with

$$C^{(2)}_{gg} = 503.664 - 29.9249\, N_L + 0.142857\, {N_L}^2 = 357.611 \, . \tag{23}$$

Similarly for the quark channel there is

$$\begin{aligned}\sigma^{(2)}_{q\bar{q}} = {} & \frac{3.60774}{\beta^2} \\ & + \frac{1}{\beta}\Big(-140.368\ln^2\beta + 32.106\ln\beta + 3.95105\Big) \\ & + 910.222\ln^4\beta - 1315.53\ln^3\beta + 592.292\ln^2\beta \\ & + 515.397\ln\beta + C^{(2)}_{q\bar{q}} \, , \end{aligned} \tag{24}$$

with

$$C^{(2)}_{q\bar{q}} = 1104.08 - 42.9666\, N_L - 4.28168\, {N_L}^2 = 782.208 \, . \tag{25}$$

We note that the $C^{(2)}$ constants have been previously obtained by us in Refs. [5] and [7] by expanding the fitting formulae from these publications. While the numbers are compatible within the estimated uncertainties, only the most recent analysis [26] provides high-precision reliable results. In the course of this study, we have also noticed that the coefficient of $\log\beta$ in the quark channel was incorrectly determined in [13].

4. Applications

A precise measurement of the total top-quark pair production cross section combined with high-accuracy theoretical predictions offers a unique possibility to constrain input parameters, such as the top-quark mass and the strong coupling constant. This approach also provides a handle on the gluon distribution function, and even allows to constrain physics beyond the SM.

4.1. Top-quark pole mass

As far as the top-quark mass is concerned, the total cross section provides a clean means of determining the pole mass. It is clear that this type of measurement will never be competitive with the best determinations of m_t, even when we take into account the ambiguities of the definition (it is unclear to what extent the kinematically reconstructed mass using Monte Carlo generators is the pole mass). On the other hand, it definitely enters the combination of results. The currently most precise analysis results in Fig. 8. This analysis allows to determine

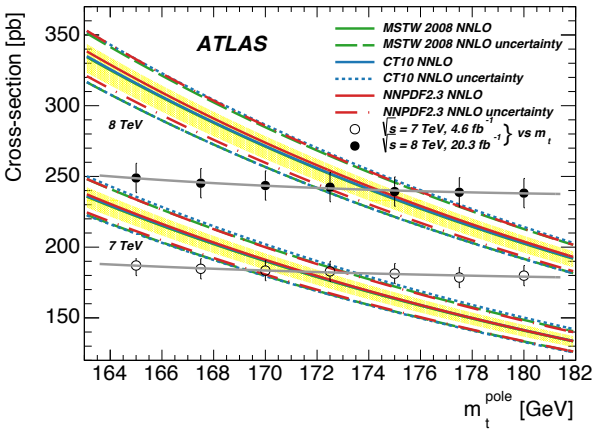

Figure 8: *Predicted NNLO+NNLL $\overline{\mathrm{tt}}$ production cross-sections at $\sqrt{s}$ = 7 TeV and $\sqrt{s}$ = 8 TeV as a function of m_t^{pole}, showing the central values (solid lines) and total uncertainties (dashed lines) with several PDF sets. The yellow band shows the QCD scale uncertainty. The measurements of $\sigma_{t\bar{t}}$ are also shown, with their dependence on the assumed value of m_t through acceptance and background corrections. Plot taken from Ref. [65].*

$$m_t^{\mathrm{pole}} = 172.9^{+2.5}_{-2.6} \text{ GeV} \, , \tag{26}$$

from a combination of results obtained at 7 and 8 TeV.

4.2. Constraints on the gluon PDF

In Ref. [66], we have performed an in-depth study of the constraints on the gluon PDF, which can inferred

from the total cross section measurement. Of course, it is clear that once differential predictions with NNLO precision will become available, the PDF can be constrained much more precisely.

Figure 9 demonstrates the strong correlation between the gluon PDF and the total cross section. In particular, the cross section probes the PDF in the range of x values from 0.1 to 0.5, where the PDF errors are in fact large.

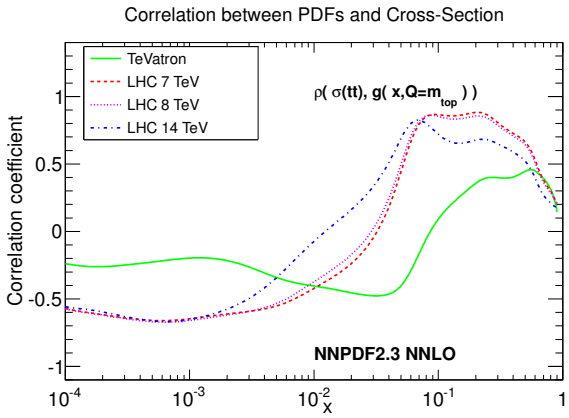

Figure 9: *The correlation between the gluon PDF from NNPDF2.3 with the total NNLO+NNLL top quark production cross sections at the Tevatron and the LHC for different center of mass energies. The correlations are computed for $Q = m_t = 173.3$ GeV. Plot taken from Ref. [66].*

The effect of including the top-quark data in the PDF fit can be made more visible by inspecting Fig. 10. The inclusion of the top-quark data leads to a reduction of the uncertainty on the PDF by about 20%.

One can also use the total top-quark pair production cross section to compare different PDF sets. This is illustrated in Fig. 11. More details on the comparisons and a discussion of the value of cross section ratios at different collider energies can be found in [66].

4.3. Constraints on light top squarks

In [67] we proposed a novel approach for constraining light top squarks. Instead of focusing on discriminating *differences* between SUSY signal and SM background, our method is based on exploiting the kinematical *similarities* between tops and stops in this region. Namely, if stop production and decays are kinematically very similar to the SM top ones, then SUSY contributions may bias SM measurements. Similar methods have been proposed for constraining new physics with W^+W^- measurements [68, 69, 70, 71, 72, 73, 74]. Therefore, we proposed to use top SM measurements and SM theoretical predictions to set limits on the stop

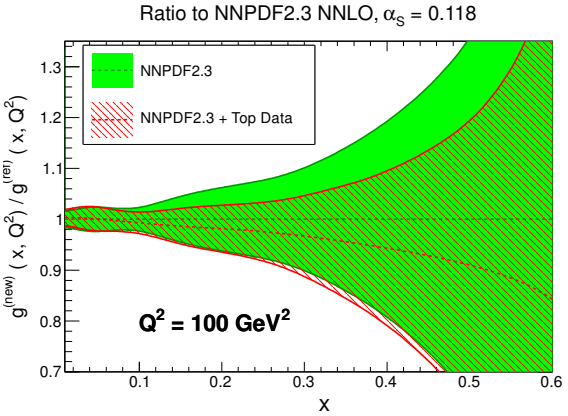

Figure 10: *The ratio of the NNPDF2.3 NNLO gluon PDF at $Q^2 = 100$ GeV^2 between the default fit and after including the Tevatron and LHC top quark cross section data. Plot taken from Ref. [66].*

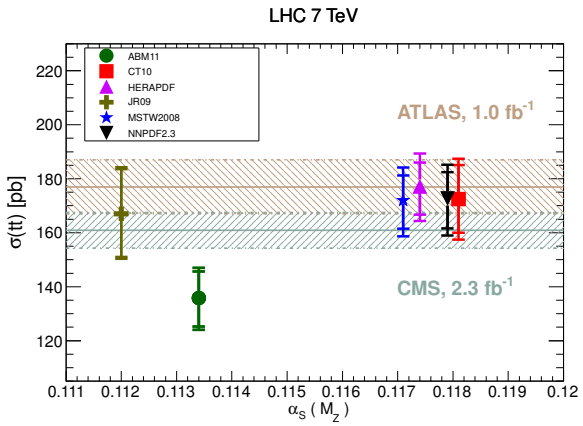

Figure 11: *The best predictions from each PDF set compared to experimental data from the LHC @ 7 TeV, as a function of the default $\alpha_s(M_Z)$ value. The inner error bar corresponds to the linear sum of PDF and scale uncertainties, while the outer error bar is the total theoretical uncertainty. Plot taken from Ref. [66].*

contamination in $t\bar{t}$ event samples. We illustrated our method by focusing on one of the most inclusive top properties, the top production cross section, $\sigma_{t\bar{t}}$. The inclusiveness has the advantage of reducing theoretical uncertainties, while our analysis profited from the recent high precision theoretical predictions.

In the presence of a SUSY contamination, the measured cross section is

$$\sigma_{t\bar{t}}^{exp} = \sigma_{t\bar{t}}(m_t)\left(1 + \frac{\epsilon_{\tilde{t}\tilde{t}^*}(m_t, m_{\tilde{t}}, m_{\chi_1^0})}{\epsilon_{t\bar{t}}(m_t)} \frac{\sigma_{\tilde{t}\tilde{t}^*}(m_{\tilde{t}})}{\sigma_{t\bar{t}}(m_t)}\right) \quad (27)$$

where with ϵ we collectively denote the efficiency and acceptances for an event to be selected by the experimental analysis. We keep the explicit mass dependence

of the various quantities, and for simplicity we include only the top squark pair production contribution. This formula gets further modified if the top is kinematically allowed to decay to a stop. Note that we assume that the stop always decays to a lighter neutralino.

For $m_{\tilde{t}} \sim m_t$, $\sigma_{\tilde{t}\tilde{t}^*} \sim 26\,\text{pb}$ at $\sqrt{s} = 7$ TeV. Taking the efficiencies $\epsilon_{t\tilde{t},\tilde{t}\tilde{t}^*}$ to be the same, and adding the theoretical and experimental uncertainties in quadrature, one naively expects to set upper bounds at 95% C.L. on $\sigma_{\tilde{t}\tilde{t}^*}$ of 45 pb and 25 pb by using the SM NLO+NLL and NNLO+NNLL predictions for $\sigma_{t\bar{t}}$ respectively. This clearly indicates that it was not possible [75] to use our proposed method before the NNLO results were available. The current constraining power of the method is illustrated in Fig. 12.

5. Forward-backward asymmetry at the Tevatron

At the Tevatron, top-quarks were produced predominantly in the hemisphere defined by the direction of the proton beam [78, 79]. This production rate difference is often referred to as Forward-Backward Asymmetry (A_{FB}). The Tevatron collider was uniquely positioned for the measurement of this asymmetry, since A_{FB} is not present at pp colliders. The persistent discrepancy [80] between the measured and predicted A_{FB}, has turned this observable into one of the most influential measurements performed at the Tevatron. Indeed, the A_{FB}-related publications by the CDF and DØ collaborations have initiated major research activity both in explaining the discrepancy with beyond the Standard Model (BSM) physics and in estimating A_{FB} within the Standard Model itself [78, 79, 81, 82, 83, 84, 85, 86, 87, 88, 89, 90].

The significance of the discrepancy between measurement and the SM theory prediction for A_{FB} has always critically hinged on the size of missing higher-order corrections. Here, we recall the calculation of the NLO QCD corrections [35] to A_{FB} in the related process $t\bar{t}j$, where a nearly -100% correction was found. Such a very large correction, if it were to also appear in $t\bar{t}$, would have had the potential of removing the discrepancy. Still, a careful analysis performed by Melnikov and Schulze [91] suggests that A_{FB} in $t\bar{t}$ is unlikely to receive very large corrections in the next order in QCD (i.e. in NNLO QCD) and is "*most likely stable against yet higher order corrections*".

In a series of papers [84, 85, 90] it was found that, unexpectedly, electroweak (EW) corrections to A_{FB} are quite large. For example, for inclusive A_{FB}, they are around 25% of the NLO QCD term. Contributions from Sudakov EW corrections have also been computed [86].

So far, the only source of information about higher-order QCD corrections to A_{FB} has been soft-gluon resummation. It was first applied at next-to-leading logarithmic accuracy (NLL) in Ref. [82] and later extended to NNLL in Ref. [83]. Further understanding of the nature of such soft emissions came in the context of parton showers and from probing them down to a single gluon emission [89]. The common finding was that, beyond NLO QCD, soft-gluon emission generates negligible corrections to inclusive A_{FB}. The natural interpretation of this result, especially when augmented with the conclusions of Ref. [91], was that the missing NNLO QCD contributions to A_{FB} in $t\bar{t}$ may be small and may not significantly affect the SM A_{FB} prediction.

An alternative approach to computing A_{FB}, based on the PMC [92] scale setting, was used in Ref. [88]. The authors derive a value for A_{FB}, which is significantly higher than the usual NLO QCD correction, in agreement with the CDF measurement. While the related BLM [93] scale setting procedure is known [94] to work well even beyond fully inclusive observables, its applicability in top production at hadron colliders is not as established. For example, the NNLO results [5, 6, 7, 8] for the terms quadratic in the number of massless quarks (N_L) in the total $t\bar{t}$ cross-section differ from those predicted within the BLM approach.

In Ref. [95], we have calculated the dominant missing correction and provided a realistic uncertainty estimate for A_{FB} in the SM. Our conclusion is that the SM prediction is under good theoretical control and agrees very well with the latest measurement – both inclusive and differential – from the DØ [96] collaboration. For inclusive A_{FB}, we find reasonable agreement with the latest measurement from the CDF collaboration [97]. In the following, we discuss our findings in more detail.

Following [97], the differential asymmetry is defined as

$$A_{FB} = \frac{\sigma^+_{\text{bin}} - \sigma^-_{\text{bin}}}{\sigma^+_{\text{bin}} + \sigma^-_{\text{bin}}} \quad , \quad \sigma^\pm_{\text{bin}} = \int \theta(\pm\Delta y)\theta_{\text{bin}} \mathrm{d}\sigma \,, \quad (28)$$

with the rapidity difference $\Delta y \equiv y_t - y_{\bar{t}}$. The binning function θ_{bin} restricts the kinematics of the $t\bar{t}$ pair to the corresponding bins in figs. 13,14,15. Setting $\theta_{\text{bin}} = 1$ in eq. (28) yields the inclusive asymmetry A_{FB}. We use two definitions for A_{FB} that are formally equivalent

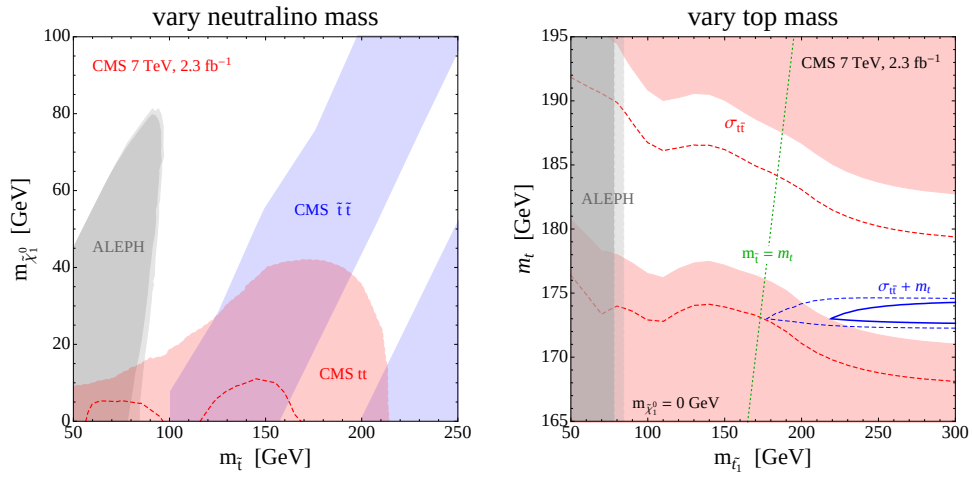

Figure 12: *Left: two dimensional 95% C.L. exclusion limits in the neutralino-stop mass plane. Our derived limits are shown in red (with expected limits shown as a dashed line), LEP limits [76] in gray while the CMS direct stop search in the light stop region [77] is shown in blue. Right: excluded regions for massless neutralino in the stop-top mass plane. Excluded region from our analysis derived using the top cross section alone (i.e. without assuming prior knowledge of the top mass) are shaded in red, while the LEP limits are shown in gray. The effect of combining the $\sigma_{t\bar{t}}$ measurement with current m_t measurements (assuming no stop contamination) is shown as a blue line. Expected limits are shown as dashed lines. For both plots we assume right-handed stop, $\tilde{t}_R$.. Plot taken from Ref. [67].*

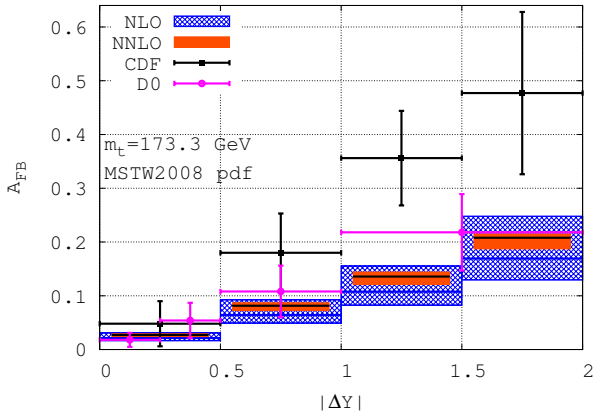

Figure 13: *The $|\Delta y|$ differential asymmetry in pure QCD at NLO (blue) and NNLO (orange) versus CDF [97] and DØ [96, 98] data. Error bands are from scale variation only. For improved readability some bins are plotted slightly narrower. The highest bin contains overflow events. Plot taken from Ref. [95].*

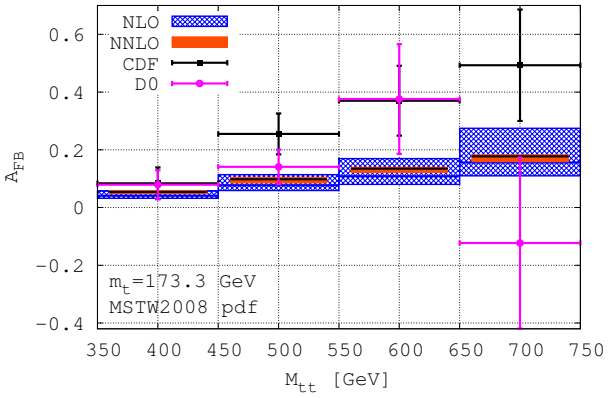

Figure 14: *As in fig. 13 but for the $M_{t\bar{t}}$ differential asymmetry. The highest bin contains overflow events and the lowest bin includes all events down to the production threshold $2m_t$. Plot taken from Ref. [95].*

through NNLO and allow for EW corrections

$$A_{FB} \equiv \frac{N_{EW} + \alpha_S^3 N_3 + \alpha_S^4 N_4 + O(\alpha_S^5)}{\alpha_S^2 D_2 + \alpha_S^3 D_3 + \alpha_S^4 D_4 + O(\alpha_S^5)} \quad (29)$$

$$= \alpha_S \frac{N_3}{D_2} + \frac{N_{EW}}{\alpha_S^2 D_2} + \alpha_S^2 \left(\frac{N_4}{D_2} - \frac{N_3 D_3}{D_2^2} \right) - \frac{N_{EW} D_3}{\alpha_S D_2^2} + O(\alpha_S^3) . \quad (30)$$

The first definition, eq. (29), uses exact results in both numerator and denominator of eq. (28), while the second, eq. (30), is the expansion of the ratio eq. (29) in powers of α_S.

In [95], we presented the differential asymmetries with the unexpanded definition (29) and without EW corrections (see figs. 13,14,15). The inclusive asymmetry, see fig. 16, was computed with both definitions (29) and (30) including EW corrections. The numerator fac-

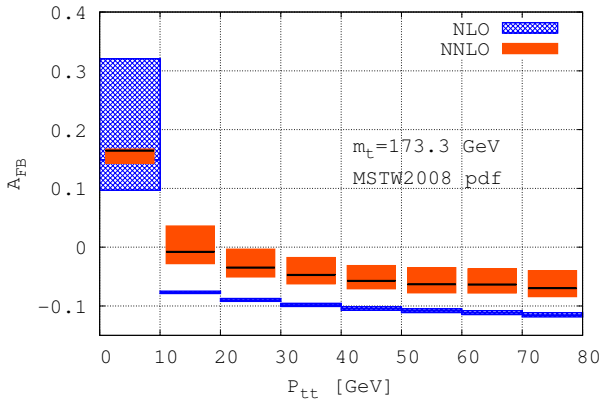

Figure 15: *As in fig. 13 but for the $P_{T,t\bar{t}}$ differential asymmetry. Plot taken from Ref. [95].*

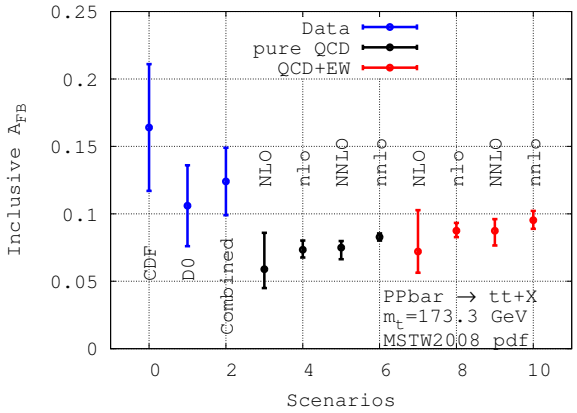

Figure 16: *The inclusive asymmetry in pure QCD (black) and QCD+EW[90] (red). Capital letters (NLO, NNLO) correspond to the unexpanded definition (29), while small letters (nlo, nnlo) to the definition (30). The CDF/DØ (naive) average is from Ref. [99]. Error bands are from scale variation only. Our final prediction corresponds to scenario 10. Plot taken from Ref. [95].*

tor $N_{\rm EW}$ has been taken from Table 2 in Ref. [90]. Only for the inclusive asymmetry we determine the scale variation by keeping $\mu_R = \mu_F$ In fig. 16 we observe that the central values of the expanded (30) and unexpanded (29) definitions of inclusive A_{FB} differ significantly at NLO but less so at NNLO. While the unexpanded definition (29) closely resembles the experimental setup, the consistency of the two definitions *within uncertainties* renders the question about the more appropriate choice largely irrelevant. We also note the small scale error for the expanded A_{FB} definition (30) in pure QCD at both NLO and NNLO, which appears too small to be realistic. The inclusion of EW corrections, however, breaks this pattern and brings the scale dependence in line with the unexpanded definition eq. (29). Therefore, following the previous literature, we chose as our final prediction $A_{FB}^{SM} = 0.095 \pm 0.007$ (scenario 10 in fig. 16) which is derived with the expanded definition (30) and includes EW [90] corrections.

In contrast to the negligible approximate NNLO QCD correction to A_{FB} implied by soft-gluon resummation [82, 83], we find that the exact NNLO QCD correction to the inclusive A_{FB} is, in fact, large. Our result brings the SM prediction for the inclusive asymmetry in perfect agreement with the measurement of the DØ collaboration and about 1.5σ below the value measured by the CDF collaboration. The predicted differential asymmetry, even without EW corrections, is in agreement with the corresponding DØ measurements.

6. Conclusions

In this proceedings we have discussed the recent advances in precision top-quark physics at hadron colliders. In particular, we have explained what methods have been used in the determination of the cross sections at next-to-next-to-leading order in QCD. Furthermore, we have shown that the measurement and theory combined at the present level of precision allow for several interesting applications. Future directions of progress concern increasingly differential analyses including top-quark decays. The projects we have described here form an excellent basis for these studies.

Acknowledgments

This work was supported by the Deutsche Forschungsgemeinschaft through the collaborative research centre SFB-TR9 “Computational Particle Physics”. We would like to thank our close collaborators Peter Bärnreuther, Paul Fiedler, David Heymes and Alexander Mitov.

References

[1] P. Nason, S. Dawson and R. K. Ellis, “The total cross-section for the production of heavy quarks in hadronic collisions”, Nucl. Phys. B **303**, 607 (1988);
[2] W. Beenakker, H. Kuijf, W. L. van Neerven and J. Smith, “QCD corrections to heavy quark production in $p\bar{p}$ collisions”, Phys. Rev. D **40**, 54 (1989);
[3] M. Czakon and A. Mitov, “Inclusive heavy flavor hadroproduction in NLO QCD: the exact analytic result”, Nucl. Phys. B **824**, 111 (2010);
[4] U. Langenfeld, S. Moch and P. Uwer, “Measuring the running top-quark mass”, Phys. Rev. D **80**, 054009 (2009);

[5] P. Bärnreuther, M. Czakon and A. Mitov, "Percent level precision physics at the Tevatron: first genuine NNLO QCD corrections to $q\bar{q} \to t\bar{t} + X$", Phys. Rev. Lett. **109** (2012) 132001;

[6] M. Czakon and A. Mitov, "NNLO corrections to top-pair production at hadron colliders: the all-fermionic scattering channels", JHEP **1212** (2012) 054;

[7] M. Czakon and A. Mitov, "NNLO corrections to top pair production at hadron colliders: the quark-gluon reaction", JHEP **1301** (2013) 080;

[8] M. Czakon, P. Fiedler and A. Mitov, "Total top-quark pair-production cross section at hadron colliders through $O(\alpha_S^4)$", Phys. Rev. Lett. **110** (2013) 252004;

[9] M. Beneke, P. Falgari and C. Schwinn, "Soft radiation in heavy-particle pair production: All-order colour structure and two-loop anomalous dimension", Nucl. Phys. B **828** (2010) 69;

[10] M. Czakon, A. Mitov and G. F. Sterman, "Threshold resummation for top-pair hadroproduction to next-to-next-to-leading log"; Phys. Rev. D **80** (2009) 074017;

[11] M. Cacciari, M. Czakon, M. Mangano, A. Mitov and P. Nason, "Top-pair production at hadron colliders with next-to-next-to-leading logarithmic soft-gluon resummation", Phys. Lett. B **710** (2012) 612;

[12] M. Czakon and A. Mitov, "Top++: a program for the calculation of the top-pair cross-section at hadron colliders", Comput. Phys. Commun. **185** (2014) 2930;

[13] M. Beneke, M. Czakon, P. Falgari, A. Mitov and C. Schwinn, "Threshold expansion of the $gg(q\bar{q}) \to Q\bar{Q} + X$ cross section at $O(\alpha_S^4)$", Phys. Lett. B **690** (2010) 483;

[14] W. Bernreuther, M. Fücker and Z. G. Si, "Weak interaction corrections to hadronic top quark pair production", Phys. Rev. D **74** (2006) 113005;

[15] J. H. Kühn, A. Scharf and P. Uwer, "Electroweak effects in top-quark pair production at hadron colliders", Eur. Phys. J. C **51** (2007) 37;

[16] M. Aldaya, "Combined top quark physics results from ATLAS and CMS", presented at ICHEP 2014, 2-9 July 2014;

[17] M. Czakon, P. Fiedler, A. Mitov and J. Rojo, "Further exploration of top pair hadroproduction at NNLO", arXiv:1305.3892 [hep-ph].

[18] S. Moch, P. Uwer and A. Vogt, "On top-pair hadro-production at next-to-next-to-leading order", Phys. Lett. B **714**, 48 (2012);

[19] S. Catani, M. Ciafaloni and F. Hautmann, "Gluon contributions to small-x heavy flavor production", Phys. Lett. B **242**, 97 (1990);

[20] J. C. Collins and R. K. Ellis, "Heavy quark production in very high-energy hadron collisions", Nucl. Phys. B **360**, 3 (1991);

[21] S. Catani, M. Ciafaloni and F. Hautmann, "High-energy factorization and small x heavy flavor production", Nucl. Phys. B **366**, 135 (1991);

[22] S. Catani, M. Ciafaloni and F. Hautmann, "High-energy factorization in QCD and minimal subtraction scheme", Phys. Lett. B **307** (1993) 147;

[23] S. Catani and F. Hautmann, "High-energy factorization and small x deep inelastic scattering beyond leading order", Nucl. Phys. B **427**, 475 (1994);

[24] R. D. Ball and R. K. Ellis, "Heavy quark production at high-energy", JHEP **0105**, 053 (2001);

[25] M. Czakon, "Tops from Light Quarks: Full Mass Dependence at Two-Loops in QCD", Phys. Lett. B **664** (2008) 307;

[26] P. Bärnreuther, M. Czakon and P. Fiedler, "Virtual amplitudes and threshold behaviour of hadronic top-quark pair-production cross sections", JHEP **1402** (2014) 078;

[27] A. Ferroglia, M. Neubert, B. D. Pecjak and L. L. Yang, "Two-loop divergences of massive scattering amplitudes in non-abelian gauge theories", JHEP **0911**, 062 (2009);

[28] C. Anastasiou and S. M. Aybat, "The One-loop gluon amplitude for heavy-quark production at NNLO", Phys. Rev. D **78**, 114006 (2008);

[29] B. Kniehl, Z. Merebashvili, J. G. Körner and M. Rogal, "Heavy quark pair production in gluon fusion at next-to-next-to-leading $O(\alpha_s^4)$ order: One-loop squared contributions", Phys. Rev. D **78**, 094013 (2008);

[30] J. G. Körner, Z. Merebashvili and M. Rogal, "Laurent series expansion of massive scalar one-loop integrals to $O(epsilson^{2})$", Phys. Rev. D **71**, 054028 (2005);

[31] Z. Bern, V. Del Duca, W. B. Kilgore and C. R. Schmidt, "The infrared behavior of one loop QCD amplitudes at next-to-next-to leading order", Phys. Rev. D **60**, 116001 (1999);

[32] S. Catani and M. Grazzini, "The soft gluon current at one loop order", Nucl. Phys. B **591**, 435 (2000);

[33] S. Catani, S. Dittmaier and Z. Trocsanyi, "One loop singular behavior of QCD and SUSY QCD amplitudes with massive partons", Phys. Lett. B **500**, 149 (2001);

[34] I. Bierenbaum, M. Czakon and A. Mitov, "The singular behavior of one-loop massive QCD amplitudes with one external soft gluon", Nucl. Phys. B **856**, 228 (2012);

[35] S. Dittmaier, P. Uwer and S. Weinzierl, "NLO QCD corrections to $t\bar{t}$ + jet production at hadron colliders", Phys. Rev. Lett. **98**, 262002 (2007);

[36] S. Dittmaier, P. Uwer and S. Weinzierl, "Hadronic top-quark pair production in association with a hard jet at next-to-leading order QCD: Phenomenological studies for the Tevatron and the LHC", Eur. Phys. J. C **59**, 625 (2009);

[37] M. Czakon, "A novel subtraction scheme for double-real radiation at NNLO", Phys. Lett. B **693**, 259 (2010);

[38] M. Czakon, "Double-real radiation in hadronic top quark pair production as a proof of a certain concept", Nucl. Phys. B **849** (2011) 250;

[39] A. Gehrmann-De Ridder, T. Gehrmann and E. W. N. Glover, "Antenna subtraction at NNLO", JHEP **0509** (2005) 056;

[40] S. Catani and M. Grazzini, "An NNLO subtraction formalism in hadron collisions and its application to Higgs boson production at the LHC", Phys. Rev. Lett. **98** (2007) 222002;

[41] G. Somogyi, Z. Trocsanyi and V. Del Duca, "Matching of singly- and doubly-unresolved limits of tree-level QCD squared matrix elements", JHEP **0506** (2005) 024;

[42] S. Frixione, Z. Kunszt and A. Signer, "Three jet cross-sections to next-to-leading order", Nucl. Phys. B **467** (1996) 399;

[43] T. Binoth and G. Heinrich, "An automatized algorithm to compute infrared divergent multiloop integrals", Nucl. Phys. B **585** (2000) 741;

[44] C. Anastasiou, K. Melnikov and F. Petriello, "A new method for real radiation at NNLO", Phys. Rev. D **69** (2004) 076010;

[45] M. Brucherseifer, F. Caola and K. Melnikov, JHEP **1304** (2013) 059;

[46] M. Brucherseifer, F. Caola and K. Melnikov, Phys. Lett. B **721** (2013) 107;

[47] R. Boughezal, F. Caola, K. Melnikov, F. Petriello and M. Schulze, JHEP **1306** (2013) 072;

[48] F. Caola, A. Czarnecki, Y. Liang, K. Melnikov and R. Szafron, arXiv:1403.3386 [hep-ph];

[49] M. Brucherseifer, F. Caola and K. Melnikov, arXiv:1404.7116 [hep-ph];

[50] R. Boughezal, K. Melnikov and F. Petriello, Phys. Rev. D **85** (2012) 034025;

[51] M. Czakon and D. Heymes, "Four-dimensional formulation of the sector-improved residue subtraction scheme", arXiv:1408.2500 [hep-ph], *to appear in Nucl. Phys. B*;

[52] R. Bonciani, A. Ferroglia, T. Gehrmann, D. Maitre and C. Studerus, "Two-loop fermionic corrections to heavy-quark

pair production: The quark-antiquark channel", JHEP **0807** (2008) 129;
[53] R. Bonciani, A. Ferroglia, T. Gehrmann and C. Studerus, "Two-loop planar corrections to heavy-quark pair production in the quark-antiquark channel", JHEP **0908** (2009) 067;
[54] R. Bonciani, A. Ferroglia, T. Gehrmann, A. Manteuffel and C. Studerus, "Two-loop leading color corrections to heavy-quark pair production in the gluon fusion channel", JHEP **1101** (2011) 102
[55] A. von Manteuffel and C. Studerus, "Massive planar and non-planar double box integrals for light N_f contributions to $gg \to t\bar{t}$", JHEP **1310** (2013) 037;
[56] R. Bonciani, A. Ferroglia, T. Gehrmann, A. von Manteuffel and C. Studerus, "Light-quark two-loop corrections to heavy-quark pair production in the gluon fusion channel", JHEP **1312** (2013) 038;
[57] M. Czakon, A. Mitov and S. Moch, "Heavy-quark production in massless quark scattering at two loops in QCD", Phys. Lett. B **651** (2007) 147;
[58] M. Czakon, A. Mitov and S. Moch, "Heavy-quark production in gluon fusion at two loops in QCD", Nucl. Phys. B **798** (2008) 210;
[59] M. Czakon, "Automatized analytic continuation of Mellin-Barnes integrals", Comput. Phys. Commun. **175** (2006) 559;
[60] H.R.P. Ferguson and D.H. Bailey, Math. of Comput. 53 (1989) 649;
[61] S. Moch and P. Uwer, Comput. Phys. Commun. **174** (2006) 759;
[62] P.N. Brown, G.D. Byrne and A.C. Hindmarsh, SIAM J. Sci. Stat. Comput. (1989) 1038;
[63] D.H. Bailey, Y. Hida and X.S. Li, Quad-double/Double-double Computation Package, http://crd.lbl.gov/~dhbailey/mpdist/;
[64] M. Czakon and P. Fiedler, "The soft function for color octet production at threshold", Nucl. Phys. B **879** (2014) 236;
[65] G. Aad *et al.* [ATLAS Collaboration], "Measurement of the $t\bar{t}$ production cross-section using $e\mu$ events with b-tagged jets in pp collisions at $\sqrt{s}$ = 7 and 8 TeV with the ATLAS detector", Eur. Phys. J. C **74** (2014) 10, 3109;
[66] M. Czakon, M. L. Mangano, A. Mitov and J. Rojo, "Constraints on the gluon PDF from top quark pair production at hadron colliders", JHEP **1307** (2013) 167;
[67] M. Czakon, A. Mitov, M. Papucci, J. T. Ruderman and A. Weiler, "Closing the stop gap", arXiv:1407.1043 [hep-ph], *to appear in Phys. Rev. Lett.*;
[68] M. Lisanti and N. Weiner, "Electroweakinos hiding in Higgs searches", Phys. Rev. D **85**, 115005 (2012);
[69] B. Feigl, H. Rzehak and D. Zeppenfeld, "New Physics backgrounds to the $H \to WW$ search at the LHC?", Phys. Lett. B **717**, 390 (2012);
[70] D. Curtin, P. Jaiswal and P. Meade, "Charginos hiding In plain sight", Phys. Rev. D **87**, no. 3, 031701 (2013);
[71] K. Rolbiecki and K. Sakurai, "Light stops emerging in WW cross section measurements?", JHEP **1309**, 004 (2013);
[72] D. Curtin, P. Jaiswal, P. Meade and P. -J. Tien, "Casting light on BSM physics with SM standard candles", JHEP **1308**, 068 (2013);
[73] D. Curtin, P. Meade and P. -J. Tien, "Natural SUSY in plain sight", arXiv:1406.0848 [hep-ph];
[74] J. S. Kim, K. Rolbiecki, K. Sakurai and J. Tattersall, "'Stop' that ambulance! New physics at the LHC?", arXiv:1406.0858 [hep-ph];
[75] Y. Kats and D. Shih, "Light stop NLSPs at the Tevatron and LHC", JHEP **1108**, 049 (2011);
[76] A. Heister *et al.* [ALEPH Collaboration], "Search for scalar quarks in e^+e^- collisions at $\sqrt{s}$ up to 209-GeV", Phys. Lett. B **537**, 5 (2002);
[77] S. Chatrchyan *et al.* [CMS Collaboration], "Search for top-squark pair production in the single-lepton final state in pp collisions at $\sqrt{s}$ = 8 TeV", Eur. Phys. J. C **73**, 2677 (2013);
[78] J. H. Kühn and G. Rodrigo, "Charge asymmetry in hadroproduction of heavy quarks", Phys. Rev. Lett. **81**, 49 (1998);
[79] J. H. Kühn and G. Rodrigo, "Charge asymmetry of heavy quarks at hadron colliders", Phys. Rev. D **59**, 054017 (1999);
[80] T. Aaltonen *et al.* [CDF Collaboration], "Evidence for a mass dependent forward-backward asymmetry in top quark pair production", Phys. Rev. D **83**, 112003 (2011);
[81] O. Antunano, J. H. Kühn and G. Rodrigo, "Top quarks, axigluons and charge asymmetries at hadron colliders", Phys. Rev. D **77**, 014003 (2008);
[82] L. G. Almeida, G. F. Sterman and W. Vogelsang, "Threshold resummation for the top quark charge asymmetry", Phys. Rev. D **78**, 014008 (2008);
[83] V. Ahrens, A. Ferroglia, M. Neubert, B. D. Pecjak and L. L. Yang, "The top-pair forward-backward asymmetry beyond NLO", Phys. Rev. D **84**, 074004 (2011);
[84] W. Hollik and D. Pagani, "The electroweak contribution to the top quark forward-backward asymmetry at the Tevatron", Phys. Rev. D **84**, 093003 (2011);
[85] J. H. Kühn and G. Rodrigo, "Charge asymmetries of top quarks at hadron colliders revisited", JHEP **1201**, 063 (2012);
[86] A. V. Manohar and M. Trott, "Electroweak sudakov corrections and the top quark forward-backward asymmetry", Phys. Lett. B **711**, 313 (2012);
[87] J. M. Campbell and R. K. Ellis, "Top-quark processes at NLO in production and decay", arXiv:1204.1513 [hep-ph];
[88] S. J. Brodsky and X. G. Wu, "Application of the Principle of Maximum Conformality to the top-quark forward-backward asymmetry at the Tevatron", Phys. Rev. D **85**, 114040 (2012);
[89] P. Skands, B. Webber and J. Winter, "QCD coherence and the top quark asymmetry", JHEP **1207**, 151 (2012);
[90] W. Bernreuther and Z. G. Si, "Top quark and leptonic charge asymmetries for the Tevatron and LHC", Phys. Rev. D **86**, 034026 (2012);
[91] K. Melnikov and M. Schulze, "NLO QCD corrections to top quark pair production in association with one hard jet at hadron colliders", Nucl. Phys. B **840**, 129 (2010);
[92] S. J. Brodsky and X. G. Wu, "Eliminating the renormalization scale ambiguity for top-pair production using the Principle of Maximum Conformality", Phys. Rev. Lett. **109**, 042002 (2012);
[93] S. J. Brodsky, G. P. Lepage and P. B. Mackenzie, "On the elimination of scale ambiguities in perturbative Quantum Chromodynamics", Phys. Rev. D **28**, 228 (1983);
[94] K. Melnikov and A. Mitov, "The photon energy spectrum in $B \to X_s + \gamma$ in perturbative QCD through $O(\alpha_S^2)$", Phys. Lett. B **620**, 69 (2005);
[95] M. Czakon, P. Fiedler and A. Mitov, "Resolving the Tevatron top quark forward-backward asymmetry puzzle", arXiv:1411.3007 [hep-ph], *submitted to Phys. Rev. Lett.*;
[96] V. M. Abazov *et al.* [D0 Collaboration], "Measurement of the forward-backward asymmetry in top quark-antiquark production in ppbar collisions using the lepton+jets channel", arXiv:1405.0421 [hep-ex];
[97] T. Aaltonen *et al.* [CDF Collaboration], "Measurement of the top quark forward-backward production asymmetry and its dependence on event kinematic properties", Phys. Rev. D **87**, 092002 (2013);
[98] Supplemental information from the DØ Collaboration: http://www-d0.fnal.gov/Run2Physics/WWW/results/final/TOP/T14D/
[99] J. A. Aguilar-Saavedra, D. Amidei, A. Juste and M. Perez-Victoria, "Asymmetries in top quark pair production", arXiv:1406.1798 [hep-ph].